Study of the Structural and Electronic Properties of Rh−N and Ru−N Clusters (N < 20) within the Density Functional Theory

ARTICLE *in* THE JOURNAL OF PHYSICAL CHEMISTRY A · OCTOBER 2009

Impact Factor: 2.69 · DOI: 10.1021/jp905188t · Source: PubMed

3 AUTHORS:

F. Aguilera-Granja
Universidad Autónoma de San Luis Potosí
150 PUBLICATIONS **1,368** CITATIONS
SEE PROFILE

Carlos Balbás
Universidad de Valladolid
136 PUBLICATIONS **2,249** CITATIONS
SEE PROFILE

Andrés Vega
Universidad de Valladolid
175 PUBLICATIONS **1,950** CITATIONS
SEE PROFILE

Study of the Structural and Electronic Properties of Rh_N and Ru_N Clusters ($N < 20$) within the Density Functional Theory

F. Aguilera-Granja*

Instituto de Física, Universidad Autónoma de San Luis Potosí, San Luis Potosí, México

L. C. Balbás and A. Vega

Departamento de Física Teórica, Atómica y Óptica, Universidad de Valladolid, Spain

Received: June 2, 2009; Revised Manuscript Received: September 29, 2009

Using the density-functional theory (DFT) with the generalized gradient approximation to exchange and correlation, we compute the geometries, electronic structure, and related properties of free-standing rhodium and ruthenium atomic clusters with sizes below 20 atoms. We explore different structural and spin isomers per size, for which we determine the interatomic distances, binding energy, magnetic moment, HOMO−LUMO gap, and electric dipole moment. For many sizes, different implementations of DFT predict different properties for the lowest-energy isomers, thus illustrating the complex nature of these 4d transition metal elements at the nanoscale. We discuss our results for rhodium clusters in the context of recent electric deflection measurements.

I. Introduction

Free-standing transition-metal (TM) atomic clusters are a matter of intense research with the goal of understanding the geometrical and electronic properties at the nanoscale as well as their interplay. This knowledge is of great relevance if those systems will be used in nanotechnology to design magnetic or catalytic devices in which the morphology plays a fundamental role. The production of size-selected, free-standing clusters in cluster beams is well-controlled at present, and the magnetic properties as a function of cluster size can be investigated through Stern−Gerlach techniques.[1−3] Molecular beam electric deflection measurements have also been carried out to characterize the electric dipole and polarizabilities of several TM clusters.[4−6]

However, the geometrical structures of free-standing clusters are more difficult to characterize, since most of the techniques used in bulk-like systems are not suitable if the cluster is not supported on a host. Therefore, in the free-standing environment, alternative techniques have emerged to find plausible geometries. In this respect, and closely related to catalysis, it is possible to take advantage of the structural dependency on the adsorption of light molecules on the surface of the cluster.[7] Other types of experiments, such as trapped ion electron diffraction[8] and infrared spectroscopy,[9] have shed light on the geometrical structure of metal clusters when combined with density functional theory (DFT) total energy calculations.

From the theoretical side, the coexistence of itinerant d electrons with delocalized sp electrons in the electronic valence of transition metals makes it difficult to treat them within simple models. If the determination of both the geometry and electronic structure is being achieved at the same level, which is desirable due to the strong interdependence of both kind of properties, DFT has been demonstrated to be a very efficient and reliable approach for many elements.

The electronic structure and magnetic properties of clusters of the non magnetic 4d elements Rh and Ru have been widely investigated from the theoretical side after the pioneering experimental work of Cox and co-workers.[2] The early theoretical studies using both semiempirical approaches and DFT did not consider full structural relaxation (due to the huge computational cost), despite interesting general trends being predicted, such as the magnetic character of small Rh and Ru clusters, in contrast with the nonmagnetic character of their bulk counterparts.[10−18] Later DFT studies, carried out considering structural relaxations, provided further details on the growth patterns and electronic properties, although the wide dispersion in results depending on the DFT flavor did not allow unambiguously proposing geometric and total spin patterns as a function of the cluster size.[19−24]

In the present work, we have calculated, using the DFT SIESTA code (Spanish Initiative for Electronic Simulation of Thousands of Atoms)[25] in the generalized gradient approximation (GGA) approximation, the geometries, electronic structure, and related properties of different isomers of Rh and Ru atomic clusters with less than 20 atoms. We have focused on the previous DFT−GGA studies that considered full structural relaxation,[19−24] against which we have benchmarked our results. We also provide results for properties that were not calculated before, such as the electric dipole and polarizability (only for some particular clusters), which we have tried to correlate, in the case of Rh, with recent electric deflection measurements[6] to finally illustrate the complex nature of these 4d TM elements at the nanoscale and the difficulty in reaching an overall agreement at the DFT level. Thus, the present work reports results obtained using another DFT−GGA implementation which we believe will be of interest for the scientific community. Since the problem still remains open, in our opinion, we hope that our work will contribute to the enrichment of the scientific discussion and to the motivation of further experimental and theoretical efforts.

* Corresponding author. E-mail: faustino@ifisica.uaslp.mx.

10.1021/jp905188t CCC: $40.75
Published on Web 10/26/2009

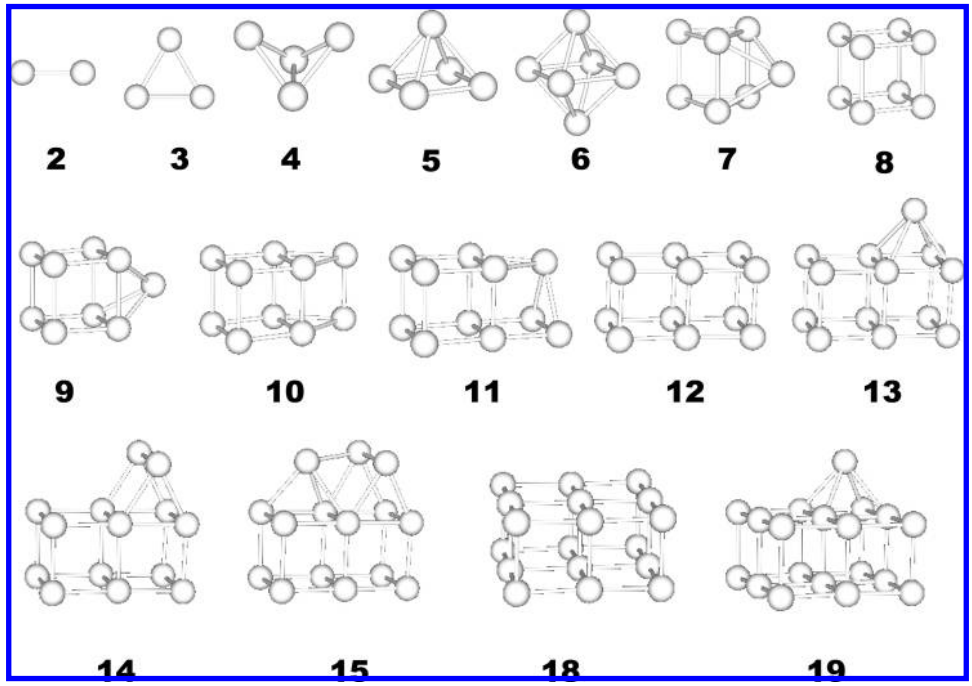

Figure 1. Illustration of the geometry of our predicted lowest-energy isomers of Rh_N clusters.

The rest of the paper is organized as follows. In Section II, we briefly describe our DFT approach. In Section III, we first compare the results obtained for the geometrical structures, binding energy, magnetic moments, and HOMO−LUMO gaps with previous DFT−GGA studies that considered full relaxation, and then we discuss the trends obtained for electrical properties (in some Rh clusters). The main conclusions are summarized at the end.

II. Theoretical Method

We have performed our calculations using the DFT approach as implemented in the code SIESTA.[25] This method employs linear combination of pseudoatomic orbitals as basis sets. The atomic core is replaced by a nonlocal norm-conserving Troullier−Martins[26] pseudopotential that is factorized in the Kleinman−Bilander form[27] and includes nonlinear core correction terms to account for the significant overlap of the core charges with the valence d orbitals. The code allows one to perform, together with the electronic calculation, structural optimization using a variety of algorithms.

In the present study, we have used the GGA to the exchange and correlation potential as parametrized by Perdew, Burke, and Ernzerhof (PBE).[28] The ionic pseudopotentials were generated using the atomic configurations $4d^n$, $5s^1$, and $5p^0$ with $n = 7$ for Ru, and $n = 8$ for Rh. The s, p and d cutoff radii were 2.40, 2.40, and 1.70 au for both elements. We have included nonlinear core corrections with a matching radius of 1.40 au in Ru and 1.20 au in Rh. We have verified that these pseudopotentials accurately reproduce the eigenvalues of different excited states of the respective isolated atoms.

Concerning the basis set and the energy cutoff to define the real space grid for numerical calculations involving the electron density, a detailed and carefull test has been performed. We have described the valence states using double-ζ polarized (DZP) basis sets with two orbitals having different radial form to describe both the 5s and the 4d shells and one orbital to describe the 5p shell. We tested for Ru_{13} a triple-ζ double polarized (TZDP) basis, that is, with three radial functions per angular momentum (instead of two, as in the DZP), as well as with double polarization of the valence s states (instead of single polarization, as in the DZP). Regarding the differences of binding energy of the different isomers with respect to the most stable one, we found that the TZDP led in general to slightly lower energy differences than does the DZP (in no more than 15 meV) and that the energetic ordering of the different isomers was unchanged. Concerning the interatomic distances, we found that the TZDP basis led to slightly shorter interatomic distances and, thus, a shorter average distance, than did the DZP basis (in no more than 0.02 Å). We have considered a 250 Ry energy cutoff to define the real space grid for numerical calculations involving the electron density and an electronic temperature of 25 meV to accelerate the self-consistency. We have tested larger cutoffs and lower electronic temperatures for particular cases, and they do not substantially modify the results.

To optimize the geometrical structures, we have performed local relaxations using the conjugate gradient algorithm starting from a large variety of initial structures having different symmetries and spin configurations (different structural and spin isomers). The structural optimization was stopped when each force component at each atom in the cluster was smaller than 5 meV/Å. For some particular clusters, we have also used the fully unconstrained version of the SIESTA code to check the possible existence of noncollinear magnetic arrangements. We have found in all cases a collinear ferromagnetic-like order.

III. Results

A. Magnetic Moment and Geometry. In Figures 1 and 2, we illustrate the geometries of our predicted lowest-energy isomers of Rh and Ru clusters, respectively. In Tables 1−3 we compare, for these lowest energy isomers, our SIESTA−GGA results with those results obtained by other groups using different DFT implementations. We focus on DFT studies that considered full structural optimization. All those studies were carried out using the GGA−PW91 approximation for the exchange and correlation potential as given by Perdew and co-workers,[29] which is known to be close to the GGA−PBE results. Nevertheless,

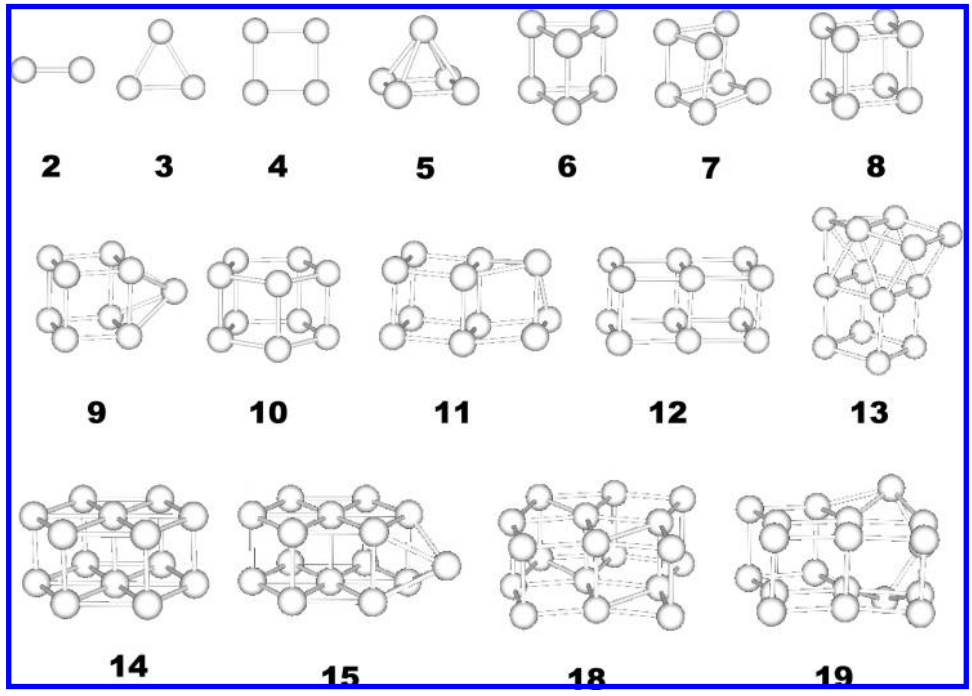

Figure 2. Illustration of the geometry of our predicted lowest energy isomers of Ru_N clusters.

TABLE 1: Average Magnetic Moment Per Atom, Binding Energy, Average Interatomic Distance and HOMO-LUMO Gap of Rh_N Clusters ($N = 2-12$) Calculated through Different DFT Implementations[a]

size	structure	$\bar{\mu}$ (μ_B)	energy (eV/atom)	av distance (Å)	gap	method
2	pair	2.00	1.798	2.27	0.41	SIESTA−PBE
		2.00	1.686	2.21	0.57	VASP−PAW−PW91[22]
		2.00	2.050	2.20	0.19	VASP−USPP−PW91[20]
		2.00	1.880	2.28	0.03	DMOL−AE−PW91[19]
3	triangle	1.67	2.375	2.49	0.30	SIESTA−PBE
		1.00	2.308	2.38	0.38	VASP−PAW−PW91[22]
		1.67	2.600		0.08	VASP−USPP−PW91[20]
		1.67	2.350	2.51	0.08	DMOL−AE−PW91[19]
4	bend rhombus	1.50	2.816	2.60	0.13	SIESTA−PBE
		1.50	3.120	2.54	0.20	VASP−USPP−PW91[20]
	tetrahedron	0.00	2.750	2.45	0.60	VASP−PAW−PW91[22]
		0.00	2.910	2.50	0.66	DMOL−AE−PW91[19]
5	square pyramid	1.00	3.076	2.54	0.11	SIESTA−PBE
		1.00	3.028	2.49	0.43	VASP−PAW−PW91[22]
		1.00	3.400	2.48	0.10	VASP−USPP−PW91[20]
		1.40	3.130	2.56	0.37	DMOL−AE−PW91[19]
6	octahedral	1.00	3.244	2.59	0.17	SIESTA−PBE
		1.00	3.204	2.54	0.20	VASP−PAW−PW91[22]
		0.00	3.250	2.59	0.40	DMOL−AE−PW91[19]
	prism	1.00	3.570	2.43	0.04	VASP−USPP−PW91[20]
7	prism + 1	1.29	3.347	2.56	0.06	SIESTA−PBE
		1.57	3.710	2.50	0.04	VASP−USPP−PW91[20]
	decahedral	1.86	3.304	2.58	0.52	VASP−PAW−PW91[22]
		1.29	3.330	2.60	0.16	DMOL−AE−PW91[19]
8	cubic	1.50	3.557	2.45	0.25	SIESTA−PBE
		1.50	3.960	2.39	0.46	VASP−USPP−PW91[21]
	octahedral + 2	1.25	3.430	2.56	0.00	VASP−PAW−PW91[22]
		1.00	3.400	2.62	0.12	DMOL−AE−PW91[19]
9	cubic + 1	1.44	3.567	2.52	0.08	SIESTA−PBE
		1.44	3.970	2.46	0.13	VASP−USPP−PW91[20]
	twin octa	1.10	3.498	2.56	0.23	VASP−PAW−PW91[22]
10	cubic + 2	1.20	3.640	2.49	0.14	SIESTA−PBE
		1.20	4.040	2.44	0.16	VASP−USPP−PW91[21]
	SAP + t + b	1.40	3.634	2.56	0.00	VASP−PAW−PW91[22]

[a] Twin octa means twin octahedral, SAP + t + b means square antiprism capped on top and bottom, and polytetra means polytetrahedral.

there is a wide dispersion in the predicted structures and spin states of many clusters. The same holds for the binding energies and, particularly, for the HOMO−LUMO gaps, even when the predicted structures match.

In the case of Rh, SIESTA gives a slightly higher binding energy, larger average distance, and smaller HOMO−LUMO gap than the all-electron VASP−PAW calculations of Futschek et al.[22] for those sizes for which both DFT codes find the same

TABLE 2: As in Table 1 but for Rh_N Clusters with $N = 13-19$[a]

size	structure	$\bar{\mu}$ (μ_B)	energy (eV/atom)	av distance (Å)	gap	method
11	cubic + 3	0.09	3.685	2.49	0.19	SIESTA−PBE
		1.00	4.050	2.46	0.17	VASP−USPP−PW91[21]
	polytetra	0.45	3.667	2.55	0.14	VASP−PAW−PW91[22]
	icosahedral − 2	0.27	3.550	2.63	0.10	DMOL−AE−PW91[19]
12	couble cubic	0.67	3.825	2.45	0.16	SIESTA−PBE
		0.67	4.190	2.40	0.26	VASP−USPP−PW91[21]
	icosahedral −1	0.62	3.590	2.67	0.07	DMOL−AE−PW91[19]
13	cubic + 1 L	0.69	3.824	2.49	0.23	SIESTA−PBE
		0.69	4.180	2.45	0.22	VASP−USPP−PW91[21]
		0.69	5.250			VASP−PAW−PW91[33]
	BBP	1.31		2.60		VASP−USPP−PW91[32]
	icosahedral	1.62	3.745	2.67	0.18	VASP−PAW−PW91[22]
		1.15	3.650	2.69	0.10	DMOL−AE−PW91[19]
14	double cubic + 2	0.57	3.871	2.48	0.12	SIESTA−PBE
		0.43	4.240	2.43	0.14	VASP−USPP−PW91[21]
15	double cubic + 3	0.60	3.889	2.54	0.14	SIESTA−PBE
		0.46	4.264	2.48	0.07	VASP−USPP−PW91[21]
18	cubic oblate	0.22	4.051	2.47	0.12	SIESTA−PBE
		0.22	4.420	2.41	0.12	VASP−USPP−PW91[21]
19	cubic oblate	0.26	4.044	2.49	0.13	SIESTA−PBE
		0.16	4.410	2.44	0.10	VASP−USPP−PW91[20]

[a] Cubic + 1 L means cubic plus one lateral atom, and BBP means bucked biplanar.

TABLE 3: As in Table 1 but for Ru_N Clusters with $N = 2 - 19$

size	structure	$\bar{\mu}$ (μ_B)	energy (eV/atom)	av distance (Å)	gap	method
2	pair	2.00	2.143	2.08	0.56	SIESTA−PBE
		2.00	2.420	2.04	0.42	VASP−PAW−PW91[24]
		2.00	2.020	2.04	0.43	VASP−USPP−PW91[23]
3	triangle	2.67	2.733	2.43	0.52	SIESTA−PBE
		2.00	3.050	2.31	0.42	VASP−PAW−PW91[24]
		2.00	2.590	2.31	0.41	VASP−USPP−PW91[23]
4	square	1.00	3.092	2.28	0.21	SIESTA−PBE
		0.00	3.580	2.18	0.45	VASP−PAW−PW91[24]
	tetrahedron	1.00	2.810	2.40	0.44	VASP−USPP−PW91[23]
5	square pyramid	0.00	3.398	2.42	0.33	SIESTA−PBE
		0.00	3.820	2.37	0.33	VASP−PAW−PW91[24]
		0.40	3.380	2.37	0.16	VASP−USPP−PW91[23]
6	prism	0.67	3.661	2.40	0.10	SIESTA−PBE
		0.34	4.100	2.33	0.06	VASP−PAW−PW91[24]
		0.67	3.680		0.08	VASP−USPP−PW91[23]
7	cubo-1	1.14	3.849	2.49	0.20	SIESTA−PBE
		0.86	4.200	2.39	0.05	VASP−PAW−PW91[24]
	octahedral + 1	0.86	3.700		0.10	VASP−USPP−PW91[23]
8	cubic	0.50	4.145	2.35	0.12	SIESTA−PBE
		0.50	4.600	2.29	0.05	VASP−PAW−PW91[24]
		0.50	4.230		0.06	VASP−USPP−PW91[23]
9	cubic +1	0.89	4.131	2.45	0.09	SIESTA−PBE
		0.89	4.580	2.38	0.05	VASP−PAW−PW91[24]
		0.50	4.180		0.16	VASP−USPP−PW91[23]
10	pentagonal rings	0.80	4.233	2.42	0.19	SIESTA−PBE
		0.80	4.270		0.07	VASP−USPP−PW91[23]
	cubic + 2	0.40	4.600	2.36	0.15	VASP−PAW−PW91[24]
11	cubic + 3	0.36	4.236	2.42	0.13	SIESTA−PBE
		0.18	4.700	2.37	0.10	VASP−PAW−PW91[24]
	pentagonal rings	0.18	4.170		0.31	VASP−USPP−PW91[23]
12	double cubic	0.00	4.398	2.40	0.18	SIESTA−PBE
		0.00	4.900	2.34	0.13	VASP−PAW−PW91[24]
		0.17	4.400		0.09	VASP−USPP−PW91[23]
13	cubic + 1 L	0.15	4.369	2.48	0.12	SIESTA−PBE
	HP −1	0.31	4.880	2.46	0.15	VASP−USPP−PW91[24]
	BBP	0.46		2.53		VASP−USPP−PW91[32]
	double cubic + t	0.46	4.370		0.07	VASP−USPP−PW91[23]
14	HP	0.43	4.479	2.50	0.10	SIESTA−PBE
		0.00	5.000	2.45	0.05	VASP−PAW−PW91[24]
15	HP + 1	0.53	4.475	2.53	0.09	SIESTA−PBE
18	cubic	0.11	4.609	2.47	0.07	SIESTA−PBE
19	cubic	0.21	5.584	2.49	0.10	SIESTA−PBE

ground state structure ($N = 2, 3, 5, 6$). Different structures are predicted otherwise. Comparing our results with the all-electron DMOL calculations of Reddy et al.,[19] the same structures are obtained again only for $N = 2, 3, 5, 6$, but with comparable binding energies and similar average interatomic distances in this case. We note that although the geometrical structures for $N = 2, 3, 5, 6$ are similar, the average magnetic moment per atom is not always the same. Discrepancies exist also between

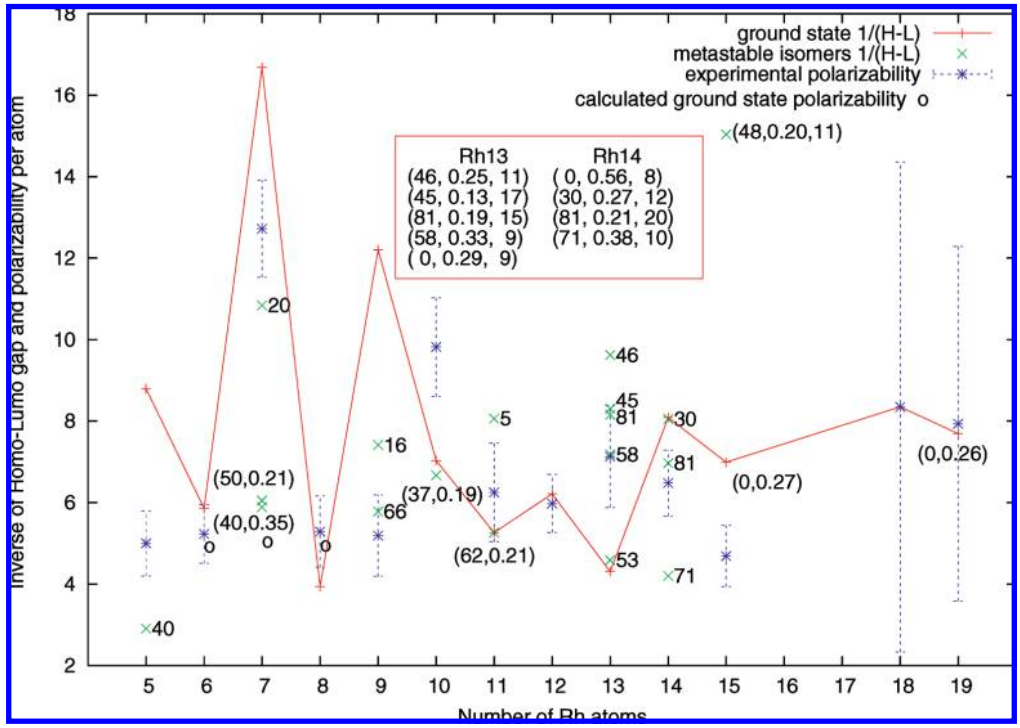

Figure 3. The inverse of the HOMO−LUMO gap (in 1/eV) calculated for the ground state (+) and for several metastable isomers (×) of Rh_N clusters ($N = 5-15$ and $18-19$) is compared to the measured static dipole polarizability per atom[6] (in Å^3) (*, with error bars). The calculated polarizability for $N = 6-8$ is also shown (o). The difference, Δ, of binding energy per atom with the ground state is given in meV for those metastable isomers with $\Delta \leq 80$ meV. For polar isomers with dipole moment $|\vec{d}| \geq 0.1$ au the values (Δ, $|\vec{d}|$) are given. In the case of Rh_{13} and Rh_{14}, these values, together with the total magnetic moment (in μ_B), are given in the inset. (The atomic unit for the dipole moment, e × Bohr, is equivalent to 2.54 D.)

the values reported by Futschek et al.[22] and by Reddy et al.,[19] even for sizes such as $N = 7-8$, 13 for which both calculations predicted the same structure (see Table 1). Comparing SIESTA with the VASP pseudopotential approach of Bae et al.,[20,21] despite the different kind of pseudopotential and basis set (ultrasoft pseudopotentials vs Troullier−Martins pseudopotentials used in SIESTA; plane waves vs localized numerical pseudoatomic orbitals in SIESTA), similar geometrical structures are predicted for all Rh clusters, with the only exception of Rh_6, and the same magnetic moment is obtained except for $N = 7$, 14, 15, 19. SIESTA always gives slightly lower binding energy and larger average distance than the plane wave calculations with ultrasoft pseudopotential.

For small Ru clusters, there are only two other DFT studies that considered full structural relaxation, one of which used the ultrasoft pseudopotential VASP code,[23] whereas the other one employed the all-electron VASP−PAW code,[24] both using a plane wave basis. SIESTA predicts the same structures as the ultrasoft pseudopotential code of Bae et al.[24] for all sizes except for $N = 13$ and departs from the structures predicted by the VASP calculations of Zhang et al.[23] only for $N = 7$, 10, 13. Therefore, there is more consensus for the Ru clusters than for the Rh ones concerning the geometrical structure. Regarding the average magnetic moment, we disagree with Bae et al.[24] for $N = 3$, 4, 6, 7, 14 (we obtained larger values) and with Zhang et al.[23] for $N = 5$, 9, 12. Concerning the binding energies and average interatomic distances, the differences between SIESTA and the ultrasoft pseudopotential code[24] are similar to those indicated previously for Rh clusters. The same holds, in general, between SIESTA and VASP for Ru clusters with less than six atoms.

We note that pseudopotential DFT approaches lead, in general, to more open structures of cubic type for these small Rh_N and Ru_N clusters than *all-electron* DFT implementations. We also note that in the case of Ru, the ultrasoft pseudopotential VASP calculations[23] depart from this trend in only two cases, Ru_7 and Ru_{10}. In a recent work, we investigated in detail the Rh and Ru clusters with 13 and 23 atoms, and we found that open arrangements of atoms were preferred, as indicated by the stability of the cubiclike structures which were, among those investigated, the ones with a lower number of bonds (or with the lowest coordination number).[30] And this question has been a long-standing issue. Thirteen-atom clusters of Pd, Rh, and Ru with radial-relaxed octahedral and icosahedral shapes were investigated by means of local spin-density calculations more than 10 years ago by Reddy and co-workers,[31] who concluded that icosahedral structures were more stable than octahedral ones and that these clusters were magnetic. Other structural shapes were tested later on. For Rh_{13} and Ru_{13}, early local spin-density calculations suggested an icosahedral ground state[11] or a fragment of the FCC crystal[22,24] or even a cagelike configuration.[20] Later on, a compact biplanar structure was also proposed as the possible ground state.[32] However, recent works support the cubiclike structures as the most probable ones,[21,33,34] like in the present work for smaller clusters. The number of localized d electrons relative to the delocalized sp ones is larger in the 4d clusters than in their 3d counterparts, and more d electrons with fewer sp electrons favor the more covalent and directional bonding of the cubic structures.

B. Electrical Properties. In Figures 3 and 4, we plot the inverse of the HOMO−LUMO gap for the lowest-energy isomers of Rh and Ru clusters, respectively, as well as for some of the metastable isomers. In the Rh clusters, we obtain negligible permanent dipole moment for the lowest energy isomers, except for $N = 13$, 14, 15, 19. Certain metastable isomers also sustain a permanent dipole moment, $\vec{d}$ (see Figure

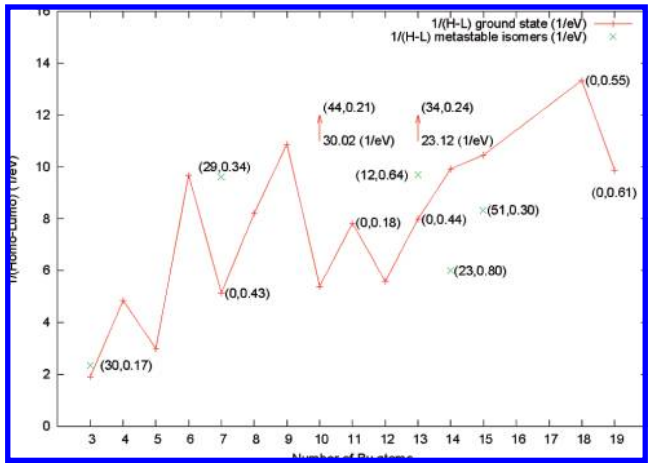

Figure 4. The inverse of the HOMO−LUMO gap (in 1/eV) calculated for the ground state (+) of Ru_N clusters ($N = 3-15$ and 18−19) and for several metastable isomers (×) with less than $\Delta \sim 50$ meV binding energy per atom than the ground state. Polar isomers with dipole moment $|\vec{d}| \geq 0.1$ au are denoted by the values (Δ, $|\vec{d}|$). The arrows at 10 and 13 number of Ru atoms indicate excited polar states with the given value for the inverse of the HOMO−LUMO gap, which is out of the plotted range, and of (Δ, $|\vec{d}|$).

3). Among them, those with $|\vec{d}| \gtrsim 0.2$ au and a binding energy difference smaller than $\sim$ 50 eV/atom with respect to the corresponding lowest isomer are illustrated in Figure 5. These are the capped octahedron of $N = 7$ (40 eV/atom less stable), the capped twin octahedron of $N = 10$ (37 eV/atom less stable), the isomers of $N = 13$, 14 with cubiclike geometries (30−46 eV/atom less stable than the lowest one that is also cubiclike), and the hexagonal-like isomer of $N = 15$ (48 eV/atom less stable) with an inverse of the HOMO−LUMO gap of 15.04 eV^{-1}. The magnetic moment of these metastable polar clusters is generally much higher than that of the ground state configuration, as shown in the inset of Figure 3 for Rh_{13} and Rh_{14} isomers.

At small enough values of the intensity of an external electric field, $\vec{F}$, the electric dipole moment, $\vec{d}$, is proportional to the external field, $\vec{d} = \alpha\vec{F}$, with α the electric polarizability, so that the Rh isomers that should have substantial electric polarizabilities could be found among the ones mentioned above. Recent electric deflection measurements by Beyer and Knickelbein for Rh clusters[6] have shown sharp peaks in the electric polarizability for Rh clusters of 7, 10 atoms and a lower and broad peak around $N = 13$. It is worth noting that none of our metastable isomers with permanent dipoles were predicted as the lowest energy isomer either by us nor by other authors who used different DFT implementations with standard flavors of the GGA. Nevertheless, the experiment of Beyer and Knickelbein provides arguments in favor of the relative stability of some of them. As we will show later in a detailed analysis for Rh_7, the binding energy of isomers as well as their electrical properties can be strongly sensitive to changes in the functional describing the exchange and correlation potential.

Concerning the Ru clusters, the lowest energy isomers of $N = 7$, 11, 13, 18, and 19 have a permanent dipole moment, $|\vec{d}| \gtrsim 0.2$ au, as well as the following metastable ones with energy difference below 50 meV/atom (illustrated in Figure 6): for $N = 3$, the isosceles triangle (30 meV/atom less stable); for $N = 7$, a spin isomer with the same cubic structure as the lowest one, but with average magnetic moment of 0.86 μ_B (30 meV/atom less stable); for $N = 10$, the cubiclike plus 2 atoms (40 meV/atom less stable); and for $N = 13$, the cubiclike with a lateral atom (10 meV/atom less stable) as well as the hexagonal (30 meV/atom less stable). Here, only three of them have been predicted as the lowest energy isomers by other authors (the isosceles triangle and the cubic isomer of Rh_7 with 0.86 μ_B/atom,[23] and the cubic-like plus 2 atoms of $N = 10$ [24]). No electric deflection experiments have been reported for Ru clusters so far, but it would be quite interesting to see up to what extent these future experiments are consistent with the above results.

We note in Figures 3 and 4 the extreme sensitivity of the HOMO−LUMO gap to the isomer geometry. For example, a difference of only 20 meV between the binding energy per atom of the capped triangular prism (prism + 1) and that of the cubo-1 isomer of Rh_7, which amounts to $\sim$0.5%, leads to a difference of $\sim$30% for the inverse of the corresponding HOMO−LUMO gap, as represented in Figure 3. In Tables 1−3, we can also observe the sensitivity of the HOMO−LUMO gap of a given structure to different types of calculations. A strong dependence on the xc-functional has also been reported for the calculated dipole polarizabilities of simple metals.[35] Therefore, the accurate determination of the polarizability of transition metal clusters is expected to be difficult within DFT.

A rough correlation between polarizability and HOMO−LUMO can be expected, since the second-order perturbation expression of the polarizability is given by $\alpha(0) = 2\Sigma'_n(|z_{n0}|^2)/(E_n - E_0)$, where z_{n0} is the matrix elements of the dipole operator, $\vec{d}$, for all single particle states ($|n>$ with energy E_n) of the system.[36] The symbol Σ' means that the highest occupied state, HOMO with energy E_0 must be excluded from the sum. Since in many cases the main contribution to that sum results from the first nonoccupied state, LUMO, it can be roughly expected that $\alpha(0) \sim (\text{HOMO} - \text{LUMO})^{-1}$. It is worth mentioning, however, that only the eigenvalue of the highest occupied orbital HOMO has a meaning within DFT, which corresponds to the adiabatic ionization potential, or chemical potential in the case of extended systems. Thus, although the static polarizability is a property of the ground state of the cluster, the calculated HOMO−LUMO value depends in an uncontrolled manner on the approximation used for the exchange-correlation functional. Nevertheless, with that caution in mind, the dipole static polarizability of Rh clusters, in $Å^3$, as measured by Beyer and Knickelbein,[6] is also depicted in Figure 3 and compared with the HOMO−LUMO values calculated for the ground state configuration of Rh_N clusters. We also provide the HOMO−LUMO of isomers with less than $\sim$80 meV binding energy difference with respect to the ground state.

As mentioned at the beginning of this section, the measured polarizability[6] shows relevant peaks at $N = 7$, 10 and a broad lower peak around 13, (those at 7 and 10 remain visible at temperatures as high as 134 K). Let us now investigate in more detail the electrical properties of the Rh_7 cluster. As we have discussed before, the capped octahedron isomer of Rh_7 has a permanent electric dipole moment, and this isomer was not predicted as the lowest energy isomer in previous DFT GGA studies. Furthermore, the electrical properties in general, and the polarizability in particular, are difficult to determine accurately within the DFT and depend on the approximation used for the exchange and correlation potential. It is for this reason that we have performed a detailed study of Rh_7 considering two unconventional flavors of the GGA. The first is the van der Waals (vdW in what follows) nonlocal energy functional of Dion et al.[37] that has been recently implemented by Soler et al.[38] in the SIESTA code. The strong dependence of the polarizability with the long-range behavior of the exchange-correlation functional has been well-established.[35] The second is our

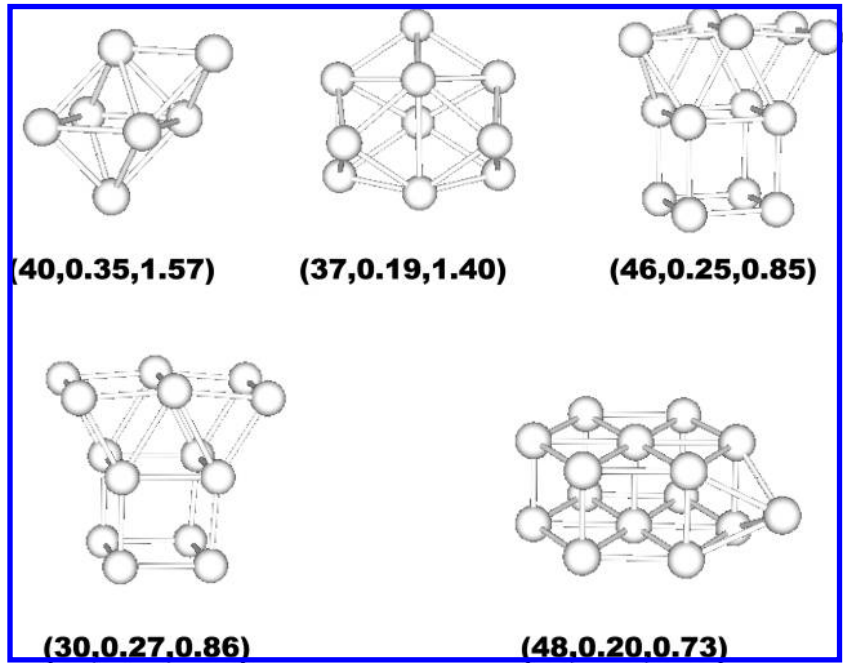

Figure 5. Geometry of the metastable isomers of Rh_N with permanent dipole moment $|\vec{d}| \gtrsim 0.2$ a.u. and a difference in binding energy smaller than ~50 meV/atom with respect to the corresponding lowest energy one. In parentheses, we give the binding energy difference (in meV/atom), the value of the dipole moment (in a.u.), and the average magnetic moment per atom (in μ_B), respectively.

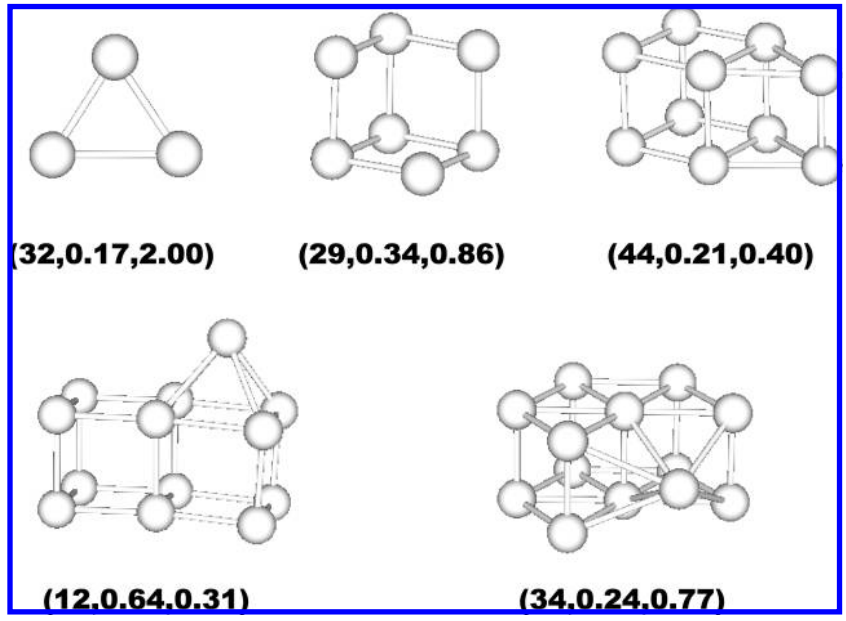

Figure 6. As in Figure 5 but for isomers of Ru_N.

implementation in SIESTA of a tightening of the Lieb−Oxford bound on the PBE functional, recently discussed by Odashima et al.,[39] and that corresponds to the ratio $\lambda = \lambda_{EL} = 2$ in $E_{xc} \geq \lambda E_x^{LDA}$ that gives the extreme low-density limit of the uniform electron liquid ($\lambda = \lambda_{LO} = 2.27$ in the standard PBE). We will refer to this xc-functional as PBM in what follows.

The static dipole polarizability of a cluster can be estimated by using the standard numerical finite field perturbation method, in which the field-dependent energy is expanded with respect to an external uniform electric field, **F**,

$$E = E^0 - d_i F_i - \frac{1}{2}\alpha_{ij} F_i F_j - \ldots \qquad (1)$$

where i, j are Cartesian coordinates and the dipole moment and the static dipole polarizability are obtained as energy derivatives, $d_i = -\partial E/\partial F_i|_{\mathbf{F}=0}$, and $\alpha_{ij} = -\partial^2 E/\partial F_i \partial F_j|_{\mathbf{F}=0}$, respectively. The external electric field values used in our calculations were (in a.u.) $F_i = 0.000, \pm 0.001, \pm 0.006, \pm 0.010$, and ± 0.020 for $i = \pm x, \pm y$, and $\pm z$. The energies calculated for these values have been fitted to a polynomial expansion to obtain the first- and second-order derivatives of energies with respect to the electric field strength. The mean polarizability is calculated as $\bar{\alpha} = \mathrm{Tr}(\alpha_{ij})/3$. This requires achieving self-consistency in both the electronic and geometrical parts for each value of the external electric field when applied along each of the three Cartesian components. This represents a huge computational task.

TABLE 4: Comparison of PBE, PBM, and vdW xc-Functionals for Several Electronic Properties of Two Rh_7 Isomers: Binding Energy Per Atom (E_b); Average Magnetic Moment Per Atom ($\bar{\mu}$); Average Polarizability Per Atom ($\bar{\alpha}$); Electric Dipolar Moment ($|\vec{d}|$); Ionization Potential (IP); Electron Affinity (EA); HOMO-LUMO Gap (H−L)

	prism+1			O_h + 1			
magnitude	PBE	PBM	vdW	PBE (11)	PBM (9)	vdW (9)	vdW (11)
E_b (eV/atom)	3.35	3.54	3.01	3.31	3.55	3.00	2.97
$\bar{\mu}$ (μ_B/atom)	1.29	1.29	1.29	1.57	1.29	1.29	1.57
$\bar{\alpha}$ (Å^3/atom)	5.06	5.31	5.24	5.39	6.42	7.46	8.54
$\|\vec{d}\|$ (Debye)	0.01	0.06	0.06	0.90	0.42	0.36	0.84
IP (eV)	6.13	6.08	6.51	6.36	6.61	6.57	6.54
EA (eV)	1.94	2.22	1.84	1.77	1.76	1.74	1.94
IP − EA (eV)	4.19	3.87	4.47	4.59	4.85	4.62	4.60
H−L (eV)	0.06	0.05	0.15	0.17	0.24	0.16	0.16

Note that two spin isomers with the vdW functional are shown for O_h + 1.

In Figure 3 the mean polarizability $\bar{\alpha}$ calculated within the PBE functional for Rh_6, Rh_7, and Rh_8 is also represented. We see that $\bar{\alpha}$ fits very well the measured value for $N = 6$ and 8, but severely fails for $N = 7$. According to Beyer and Knickelbein,[6] the deflection profile for Rh_7 is characteristic of clusters with a substantial permanent dipole moment, which was estimated to be 0.24 D using the adiabatic rotor model.[6] In other words, the isomer O_h + 1 of Rh_7 with a permanent dipole moment (see Figure 5) can be expected to have a significant charge transfer among Rh atoms, thus contributing substantially to the average atomic polarizability.[40] Our calculated dipole moment for Rh_7 is smaller than 0.06 D for all the low-lying-energy isomers, except for the capped octahedron (O_h + 1) which is 0.90 (0.82) D for the state with total spin moment 11 (9) μ_B. The state with total spin moment 9 μ_B, is only 25 meV per atom less stable than the one with 11 μ_B.

In Table 4, we report the values of relevant properties related to $\bar{\alpha}$; namely, the absolute value of the dipole moment, $|\vec{d}|$; the adiabatic ionization potential, IP; the adiabatic electron affinity, EA; the difference, IP − EA (known as hardness); and the HOMO−LUMO gap. These values were obtained with the PBE, PBM, and vdW xc-functionals for the ground state (prism + 1), which has spin moment = 9 μ_B for the three functionals, as well as for the capped octahedron (O_h + 1) isomer, which has spin moment of 9 μ_B for PBM and vdW functionals and 11 μ_B for the PBE functional. To compare with the PBE results as well as to show the correlation between magnetic moment and polarizability, we also quote in Table 4 the value $\bar{\alpha}$ (vdW) for the isomer of O_h + 1 with spin moment = 11 μ_B. First, we see that the ground state of Rh_7 for the PBM functional is the capped octahedron with only 10 meV more binding energy per atom than the capped prism configuration. This result is opposite to the one obtained with the PBE and vdW functionals. For the vdW functional, the capped prism has only 10 (40) meV more binding energy per atom than the capped octahedron with spin 9 (11) μ_B. Note that the magnetic moment is the same for the prism + 1 and O_h + 1 isomers within the three functionals, except for O_h + 1 within PBE (11 μ_B instead of 9 μ_B). The mean polarizability, $\bar{\alpha}$, has been calculated keeping the spin fixed to that of the configuration at zero external field. We see that the PBM and vdW functionals give a higher value of $\bar{\alpha}$ than the PBE functional. On the other hand, for the three xc-functionals, $\bar{\alpha}$ is higher for the O_h + 1 isomer than for the nonpolar prism + 1, as expected from the minimum polarizability principle.[41] Thus, $\bar{\alpha}$ (vdW) is considerably larger for the O_h + 1 polar configuration than for the nonpolar prism + 1 with the same spin moment, 9 μ_B, but still smaller than for the O_h + 1 isomer with magnetic moment 11 μ_B. The PBM and vdW approaches improve the prediction of the polarizability of Rh_7 compared to the PBE xc-functional. In particular, for the O_h + 1 isomer with spin moment 11 μ_B, the vdW functional correlates better with the measured polarizability,[6] as can be seen in Table 4. The electric dipole predicted by PBE and vdW for the $\mu = 11$ μ_B O_h + 1 isomer are not too different, however (0.90 and 0.84 D, respectively). For the spin isomer with total spin moment of 9 μ_B, the vdW functional gives the best result for the dipole moment (0.36 D) versus the experimental value (0.24 D).

In Table 4, we also report the values of the ionization potential, IP, the electron affinity, EA, the difference IP − EA, and the HOMO−LUMO gap, respectively. The EA and HOMO−LUMO gap of neutral clusters can be obtained experimentally by means of photoelectron spectroscopy[42] on the anionic specimen. As long as the values of IP and EA are calculated as the difference of the total energy of the relaxed neutral and charged clusters (cation and anion, respectively, for IP and EA), these properties are well-defined within DFT. If the calculated HOMO and LUMO eigenvalues of a given configuration were to be considered as realistic estimations for all xc-functionals, a correlation between the HOMO−LUMO gap and the IP-EA values should be expected. This is roughly verified for the ground state, as shown in Table 4.

IV. Summary

We have calculated, using the DFT in the GGA approximation as implemented in the SIESTA code, the geometries, electronic structure, and related magnetic and electrical properties of different isomers of Rh and Ru clusters with less than 20 atoms. We have compared the geometries, binding energies, average magnetic moments, and HOMO−LUMO gap of our predicted lowest-energy isomers with the results obtained by other groups using different DFT implementations with conventional GGA functionals, either all-electron or pseudopotential-based ones. There is, in general, a wide dispersion in the predicted structures and spin states of many of these clusters. The same holds for the binding energies and, particularly, for the HOMO−LUMO gap, even when the predicted structures match. The pseudopotential DFT approaches lead, in general, to more open structures of cubic type for these small Rh_N and Ru_N clusters than the all-electron DFT implementations.

We have also determined some properties that were not calculated before, such as the electric dipole and static polarizability (in Rh_6, Rh_7, Rh_8), which we have tried to correlate with recent electric deflection measurements in rhodium clusters.[6] A rough correlation has been found between the polarizability and the inverse of the HOMO−LUMO gap. A detailed study of Rh_7, which has a polar metastable isomer (capped octahedron), has been performed considering two unconventional flavors of the GGA. These two are the nonlocal van der Waals energy functional (vdW) and a low-density-limit tightening of the Lieb−Oxford bound on the PBE functional. We have found that this polar isomer (capped octahedron) is the ground state of the PBM xc-functional with only 10 meV more binding energy per atom than the capped prism configuration. Both the vdW and the PBM xc-functionals improve the prediction of the polarizability of the Rh_7 isomer, particularly the vdW functional for the capped octahedron with total spin moment of 11 μ_B. Thus, the experimentally observed peak in the polarizability of Rh_7, together with our results, provides arguments in favor of the capped octahedron structure of Rh_7 with total spin moment of 11 μ_B.

The EA and HOMO−LUMO gap of neutral clusters can be obtained experimentally by means of photoelectron spectroscopy[42] on the anionic specimen. This will provide, together with the polarizability, additional information to set up the ground state and eventually to select the adequate xc-functional to study the electronic properties of transition metal clusters. Other types of experiments, such as trapped ion electron diffraction[7] and infrared spectroscopy,[9] have shed light on the geometrical structure of metal clusters when combined with DFT total energy calculations. Nevertheless, currently practiced DFT cannot predict accurately the ground state geometry of a cluster if its isomers lie within an energy range of ~ 0.2 eV. Thus, comparison with several types of experiments is needed to identify the preferred geometry and to select the most accurate xc-functional. Because rhodium is an element of great interest in catalysis, the determination of its morphology, electronic structure and related magnetic and electrical properties at the nanoscale is a challenge.

Acknowledgment. We acknowledge financial support from the Spanish Ministry of Science and Innovation (Project FIS2008-02490) in conjunction with the European Regional Development Fund, and by the Junta de Castilla y León (Project no. GR120). F.A.-G. acknowledges financial support from PROMEP-SEP-CA230, CONACyT 2005-50650, C09-FAI-03-27.27 UASLP, and computer resources from the Centro Nacional de Supercomputo (CNS) from the IPICyT, San Luis Potosí, S.L.P., México. Thanks are due to José Soler for providing us with the Siesta code implementation of the van der Walls functional.

References and Notes

(1) Billas, I. M. L.; Becker, J. A.; Chaterline, A.; de Heer, W. A. *Phys. Rev. Lett.* **1993**, *71*, 4067.
(2) Cox, A. J.; Louderback, J. G.; Apsel, S. E.; Bloomfield, L. A. *Phys. Rev. B* **1994**, *49*, 12295.
(3) Payne, F. W.; Jiang, W.; Bloomfield, L. A. *Phys. Rev. Lett.* **2006**, *97*, 193401.
(4) Knickelbein, M. B. *J. Chem. Phys.* **2001**, *115*, 5957. *J. Chem. Phys.* **2003** *118*, 6230.
(5) Moro, R.; Xu, X.; Yin, S.; de Heer, W. A. *Science* **2003**, *300*, 1265.
(6) Beyer, M. K.; Knickelbein, M. B. *J. Chem. Phys.* **2007**, *126*, 104301.
(7) Parks, E. K.; Nieman, G. C.; Kerns, K. P.; Riely, S. J. *J. Chem. Phys.* **1997**, *107*, 1861.
(8) Xing, X.; Yoon, B.; Landman, U.; Parks, J. H. *Phys. Rev. B* **2006**, *74*, 165423.
(9) Gruene, P.; Rayner, D. M.; Redlich, B.; van der Meer, A. F. G.; Lyon, J. T.; Meijer, G.; Fielicke, A. *Science* **2008**, *321*, 674.
(10) Galicia, R. *Rev. Méx. Fís.* **1985**, *32*, 51.
(11) Jinlong, Y.; Toigo, F.; Kelin, W. *Phys. Rev. B* **1994**, *50*, 7915.
(12) Piveteau, B.; Desjonquéres, M. C.; Olés, A. M.; Spanjaard, D. *Phys. Rev. B* **1996**, *53*, 9251.
(13) Zhang, G. W.; Feng, Y. P.; Ong, C. K. *Phys. Rev. B* **1996**, *54*, 17208.
(14) Guirado-López, R.; Spanjaard, D.; Desjonquéres, M. C. *Phys. Rev. B* **1998**, *57*, 6305.
(15) Chien, Ch.-H.; Blaisten-Barojas, E.; Pederson, M. R. *Phys. Rev. A* **1998**, *58*, 2196.
(16) Kaiming, D.; Jinlong, Y.; Chuanyun, X.; Kelin, W. *Phys. Rev. B* **1996**, *54*, 2191.
(17) Guirado-López, R.; Spanjaard, D.; Desjonquéres, M. C.; Aguilera-Granja, F. *J. Magn. Magn. Mater.* **1998**, *186*, 214.
(18) Aguilera-Granja, F.; Rodríguez-López, J. L.; Michaelian, K.; Berlanga-Ramírez, E. O.; Vega, A. *Phys. Rev. B* **2002**, *66*, 224410.
(19) Reddy, B. V.; Nayak, S. K.; Khanna, S. N.; Rao, B. K.; Jena, P. *Phys. Rev. B* **1999**, *59*, 5214.
(20) Bae, Y. C.; Osanai, H.; Kumar, V.; Kawazoe, Y. *Phys. Rev. B* **2004**, *70*, 195413.
(21) Bae, Y. C.; Kumar, V.; Osanai, H.; Kawazoe, Y. *Phys. Rev. B* **2005**, *72*, 125427.
(22) Futschek, T.; Marsman, M.; Hafner, J. *J. Phys.: Condens. Matter* **2005**, *17*, 5927.
(23) Zhang, W.; Zhao, H.; Wang, L. *J. Phys. Chem. B* **2004**, *108*, 2140.
(24) Bae, Y. C.; Osanai, H.; Kumar, V.; Kawazoe, Y. *Mater. Trans.* **2005**, *46*, 159.
(25) Soler, J. M.; Artacho, E.; Gale, J. D.; García, A.; Junquera, J.; Ordejon, P.; Sánchez-Portal, D. *J. Phys.: Condens. Matter* **2002**, *14*, 2745.
(26) Troullier, N.; Martins, J. L. *Phys. Rev. B* **1991**, *43*, 1993.
(27) Kleinman, L.; Bilander, D. M. *Phys. Rev. Lett.* **1982**, *48*, 1425.
(28) Perdew, J. P.; Burke, K.; Ernzerhof, M. *Phys. Rev. Lett.* **1996**, *77*, 3865.
(29) Perdew, J. P. In *Electronic Structure of Solids 1*; Ziesche, P., Eschrig, H., Eds.; Academic-Verlag: Berlin, 1991, p 11.
(30) Aguilera-Granja, F.; García-Fuente, A.; Vega, A. *Phys. Rev. B* **2008**, *78*, 134425.
(31) Reddy, B. V.; Nayak, S. K.; Dunlap, B. I. *Phys. Rev. Lett.* **1993**, *70*, 3323.
(32) Chang, C. M.; Chou, M. Y. *Phys. Rev. Lett.* **2004**, *93*, 133401.
(33) Wang, L. L.; Johnson, D. D. *Phys. Rev. B* **2007**, *75*, 235405.
(34) Zhang, W.; Zhao, H.; Wang, L. *J. Phys. Chem. B* **2004**, *108*, 2140.
(35) Rubio, A.; Balbás, L. C.; Serra, Ll.; Barranco, M. *Phys. Rev. B* **1990**, *42*, 10950.
(36) Bransden, B. H.; Joachain, C. J. *Atomic and Molecular Physics*: Prentice Hall: New York, 2003.
(37) Dion, M.; Rydberg, H.; Schröder, E.; Langreth, D. C.; Lundqvist, B. I. *Phys. Rev. Lett.* **2004**, *92*, 246401.
(38) Román-Pérez, G.; Soler, J. M. *Phys. Rev. Lett.* **2009**, *103*, 096102.
(39) Odashima, M. M.; Capelle, K. *Phys. Rev. A* **2009**, *79*, 062515.
(40) Guillaume, M.; Champagne, B.; Bégué, D.; Pouchan, C. *J. Chem. Phys.* **2009**, *130*, 134715.
(41) Chattaraj, P. K.; Sengupta, S. *J. Phys. Chem. A* **1996**, *100*, 16126.
(42) Lau, J. T.; Rittmann, J.; Zamudio-Bayer, V.; Vogel, M.; Hirsch, K.; Klar, Ph.; Lofink, F.; Möller, T.; Issendorff, B. v. *Phys. Rev. Lett.* **2008**, *101*, 153401.

JP905188T